

# Conformal Graph Prediction with Z-Gromov Wasserstein Distances

Gabriel Melo<sup>1</sup>Thibaut de Saivre<sup>1</sup>Anna Calissano<sup>2</sup>Florence d'Alché-Buc<sup>1</sup><sup>1</sup>LTCI, Télécom Paris, Institut Polytechnique de Paris, Palaiseau, France<sup>2</sup>Department of Statistical Science, University College London, London, UK

## Abstract

Supervised graph prediction addresses regression problems where the outputs are structured graphs. Although several approaches exist for graph-valued prediction, principled uncertainty quantification remains limited. We propose a conformal prediction framework for graph-valued outputs, providing distribution-free coverage guarantees in structured output spaces. Our method defines nonconformity via the Z-Gromov-Wasserstein distance, instantiated in practice through Fused Gromov-Wasserstein (FGW), enabling permutation invariant comparison between predicted and candidate graphs. To obtain adaptive prediction sets, we introduce Score Conformalized Quantile Regression (SCQR), an extension of Conformalized Quantile Regression (CQR) to handle complex output spaces such as graph-valued outputs. We evaluate the proposed approach on a synthetic task and a real problem of molecule identification.

## 1 INTRODUCTION

Motivated by various applications such as molecular identification [Nguyen et al., 2019] in chemistry or scene understanding in computer vision [Shit et al., 2022], Supervised Graph Prediction (SGP) has recently attracted a growing interest in Machine Learning. This task consists in learning a predictive model that maps an input variable of any modality (text, image, tabular or distributional) to a target graph of arbitrary size. Approaches proposed in the literature leverage surrogate regression in graph representation spaces [Brouard et al., 2016] or end-to-end learning [Shit et al., 2022, Yang et al., 2024, Krzakala et al., 2024] that boils down to graph-valued regression [Calissano et al., 2022]. However, none of these approaches provides the user with confidence sets which raises a significant risk for discovery

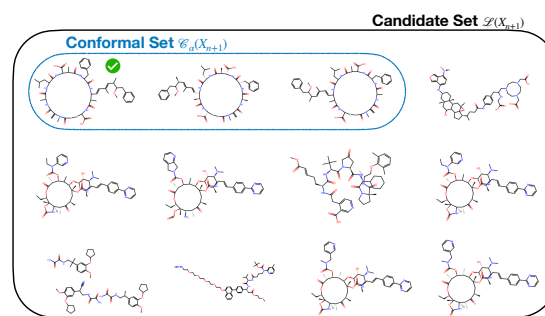


Figure 1: Conformal metabolite prediction set at 90% marginal coverage for molecule identification on MassSpec-Gym. The green check-mark denotes the ground-truth.

or identification, especially when experimental validation of the results is costly.

Uncertainty quantification for graph-valued data aims to produce a set of plausible graphs rather than a single prediction. Although random graph models are well studied [Frieze and Karoński, 2015], parametric approaches are often unrealistic in practice, especially for attributed graphs. Non-parametric methods therefore provide a more flexible alternative.

In this paper, we choose the agnostic, distribution free, and post-training framework of Conformal Prediction (CP). Conformal Prediction [Shafer and Vovk, 2008, Fontana et al., 2023] provides finite-sample coverage guarantees under minimal assumptions, requiring only exchangeability of the data, and can be applied on top of any pre-trained predictor without modifying the training procedure. Extending CP to graph-valued outputs raises several fundamental challenges. Even in the multivariate Euclidean setting, constructing informative conformal sets is known to be difficult due to the curse of dimensionality and the lack of natural orderings [Dheur et al., 2025, Kondratyev et al., 2025, Thurin et al., 2025]. These challenges are amplified in the graph setting, where outputs live in a highly structured, non-Euclidean, and combinatorial space.

For a graph with attributes on nodes and edges, uncertainty can revolve around the uncertainty at the global level, providing a conformal set made of a set of graphs with more or less different structure, or at a local level, measuring uncertainty at the level of the nodes and edges attribute. In this paper, we opt for a global framework. This choice is also supported by a specific focus on molecular identification tasks, where only a specific amount of configurations are possible.

A central challenge is therefore the choice of a suitable non-conformity score, which determines the structure and informativeness of the resulting conformal sets. Since graphs are defined up to node permutation, one must either work in the quotient space or use a permutation-invariant discrepancy. We adopt Optimal Transport distances, namely Gromov–Wasserstein and its variants, to define permutation-invariant scores and extend Conformal Prediction to graph-valued outputs with validity in the quotiented graph space.

We focus on Supervised Graph Prediction settings where each input is associated with a finite, input-dependent candidate set of graphs, as commonly assumed in structured output prediction and molecular identification.

Standard conformal prediction relies on a single global threshold, implicitly assuming homogeneous uncertainty across inputs. To account for input-dependent variability, we introduce *Score Conformalized Quantile Regression* (SCQR), which calibrates conditional quantiles of the non-conformity score instead of a global cutoff. SCQR yields locally adaptive conformal sets while preserving marginal coverage guarantees.

Finally we empirically test our novel framework on a synthetic image-to-graph task and metabolite identification from mass spectra, assessed on MassSpecGym, a recent benchmark in metabolomics [Bushuiev et al., 2024].

In short, our contributions include:

- a framework for Conformal Graph Prediction based on  $Z$ -Gromov-Wasserstein non-conformity scores and the proof of its validity in quotiented graph spaces.
- a locally adaptive variant, Score Conformalized Quantile Regression (SCQR), with proven marginal coverage.
- a set of numerical experiments showing the effectiveness and the versatility of the framework on a synthetic image-to-graph task and a real molecule prediction problem.

## 2 RELATED WORK

**Prediction Models for Graphs.** We consider supervised models whose outputs are graphs, including barycenter-based methods [Brogat-Motte et al., 2022, Yang et al., 2024],

graph regression [Calissano et al., 2022], deep end-to-end predictors [Krzakala et al., 2024, Shit et al., 2022], and graph-level autoencoders [Krzakala et al., 2025]. In molecular applications, graphs may also be predicted indirectly via SMILES representations [Wang et al., 2026, Zhang et al., 2025]. Our framework is model-agnostic and applies to both direct graph predictors and SMILES-based pipelines. In experiments, we use ANY2GRAPH and SPECBRIDGE as representative instances.

**Conformal Prediction for Graphs.** Recent efforts have extended CP to non-Euclidean domains. For node-level tasks, Huang et al. [2023] introduced conformalized GNNs, establishing the importance of permutation invariance in base predictors, while [Lunde et al., 2025] defined a node based CP sets. Zhang et al. [2024] proposed a general framework for conformal structured prediction, constructing structured prediction sets via implicit representations, e.g., directed acyclic graphs for hierarchical labels. Closer to our setting, Calissano et al. [2024] developed CP sets for populations of unlabeled graphs, utilizing quotient spaces to handle the lack of node correspondence. Our work extends these concepts to graphs with categorical *attributes* on nodes. In addition, by adopting the  $Z$ -Gromov-Wasserstein distance, we work in a permutation invariant setting.

## 3 BACKGROUND

We begin by reviewing the two central components of our framework: conformal prediction and the  $Z$ -Gromov-Wasserstein ( $Z$ -GW) distance, a metric on metric measure spaces, under which graphs naturally appear as an example of discrete metric measure spaces.

**Notation** Let  $\Sigma_n := \{a \in \mathbb{R}_+^n : \sum_{i=1}^n a_i = 1\}$  denote the probability simplex, and let  $\sigma_n := \{P \in \{0, 1\}^{n \times n} : P\mathbf{1}_n = \mathbf{1}_n, P^\top \mathbf{1}_n = \mathbf{1}_n\}$  be the set of permutation matrices, where  $\mathbf{1}_n \in \mathbb{R}^n$  denotes the all-ones vector. For finite sets  $\mathcal{X} = \{x_1, \dots, x_n\}$  and  $\mathcal{Y} = \{y_1, \dots, y_m\}$ , any discrete probability measures  $\mu \in \mathcal{P}(\mathcal{X})$  and  $\nu \in \mathcal{P}(\mathcal{Y})$  can be written as  $\mu = \sum_{i=1}^n a_i \delta_{x_i}$  and  $\nu = \sum_{j=1}^m b_j \delta_{y_j}$  with  $a \in \Sigma_n$  and  $b \in \Sigma_m$ . We identify admissible couplings  $\pi \in \Pi(\mu, \nu)$  with nonnegative matrices  $\pi \in \mathbb{R}_+^{n \times m}$  satisfying  $\pi \mathbf{1}_m = a, \pi^\top \mathbf{1}_n = b$ . When both measures are uniform, i.e.  $\mu(\{x_i\}) = \nu(\{y_j\}) = \frac{1}{n}$  for all  $i, j$  and  $n = m$ , the set  $\Pi(\mu, \nu)$  coincides with the Birkhoff polytope.

### 3.1 CONFORMAL PREDICTION

**Definition 3.1** (Exchangeability). *A sequence of random variables  $(Z_1, \dots, Z_{n+1})$  taking values in a measurable space  $\mathcal{Z}$  is said to be exchangeable if, for any permutation  $\sigma$  of  $\{1, \dots, n+1\}$  and for any  $(z_1, \dots, z_{n+1}) \in \mathcal{Z}^{n+1}$ ,  $\mathbb{P}(Z_1 = z_1, \dots, Z_{n+1} = z_{n+1}) = \mathbb{P}(Z_{\sigma(1)} =$*

$$z_1, \dots, Z_{\sigma(n+1)} = z_{n+1}.$$

Conformal Prediction (CP) provides finite-sample, distribution-free guarantees on the coverage of prediction sets. In the regression setting, we observe exchangeable pairs  $(X_i, Y_i)$  and have a pre-trained base predictor  $f_\theta : \mathcal{X} \rightarrow \mathcal{Y}$ . The framework relies on a *nonconformity score* function  $s : \mathcal{X} \times \mathcal{Y} \rightarrow \mathbb{R}$  that measures the discrepancy between the target  $y$  and the prediction  $f_\theta(x)$ . For standard real-valued regression, a typical choice is the absolute residual:

$$s(x, y) = |y - f_\theta(x)|. \quad (1)$$

Given a held-out calibration set  $\mathcal{D}_{\text{cal}} = \{(X_i, Y_i)\}_{i=1}^n$ , we compute the scores  $R = \{R_1, \dots, R_n\}$  where  $R_i = s(X_i, Y_i)$ . We then compute the adjusted empirical quantile:

$$\hat{q}_{1-\alpha} = \text{Quantile} \left( \{R_i\}_{i=1}^n, \frac{[(n+1)(1-\alpha)]}{n} \right). \quad (2)$$

For a new input  $X_{n+1}$ , the conformal prediction set is defined as:

$$\mathcal{C}(X_{n+1}) = \{y \in \mathcal{Y} : s(X_{n+1}, y) \leq \hat{q}_{1-\alpha}\}. \quad (3)$$

By exchangeability of the calibration and test samples, the nonconformity scores  $\{R_i\}_{i=1}^{n+1}$  with  $R_i = s(X_i, Y_i)$  form an exchangeable sequence. Consequently, the rank of  $R_{n+1}$  among  $\{R_i\}_{i=1}^{n+1}$  is uniformly distributed, which implies the marginal coverage guarantee [Vovk et al., 2005]

$$\mathbb{P}(Y_{n+1} \in \mathcal{C}(X_{n+1})) \geq 1 - \alpha,$$

without any assumptions on the data distribution or the accuracy of the predictor. We refer to Angelopoulos et al. [2023], Shafer and Vovk [2008] for more details on conformal prediction.

**Conformalized Quantile Regression** To extend standard conformal prediction to better handle heteroscedasticity, Conformalized Quantile Regression (CQR) [Romano et al., 2019] improves the conformal framework by leveraging quantile regression [Koenker and Bassett, 1978] to construct input-adaptive prediction intervals. Instead of relying on a fixed, globally calibrated residual, CQR employs two base models,  $\hat{\psi}_{\alpha/2}(x)$  and  $\hat{\psi}_{1-\alpha/2}(x)$ , trained to estimate the lower and upper  $(\alpha/2, 1 - \alpha/2)$  quantiles of the conditional distribution  $Y|X = x$ . The nonconformity score is then defined as  $s(x, y) = \max\{\hat{\psi}_{\alpha/2}(x) - y, y - \hat{\psi}_{1-\alpha/2}(x)\}$ , which measures the signed distance of the target to the boundaries of the predicted interval. By computing the  $(1 - \alpha)$ -th quantile of these scores,  $\hat{q}_{1-\alpha}$ , on a calibration set, the resulting prediction intervals  $\mathcal{C}(x) = [\hat{\psi}_{\alpha/2}(x) - \hat{q}_{1-\alpha}, \hat{\psi}_{1-\alpha/2}(x) + \hat{q}_{1-\alpha}]$  achieve valid marginal coverage while dynamically adjusting their width to account for local uncertainty in the data.

## 3.2 Z-GROMOV WASSERSTEIN DISTANCE

To measure discrepancies between structured outputs such as graphs, which will later serve as the basis for conformal scoring, we work in the space of  $Z$ -networks equipped with the  $Z$ -Gromov–Wasserstein distance.

**Definition 3.2** (Metric Measure Spaces). *A metric measure space (mm-space) is defined as triple  $(\mathcal{X}, d_{\mathcal{X}}, \mu_{\mathcal{X}})$ , where  $(\mathcal{X}, d_{\mathcal{X}})$  is a compact metric space and  $\mu_{\mathcal{X}}$  is a Borel probability measure on  $\mathcal{X}$  with  $\mu_{\mathcal{X}}(\mathcal{X}) = 1$  and full support,  $\text{supp}(\mu_{\mathcal{X}}) = \mathcal{X}$ .*

Gromov–Wasserstein (GW) distances were introduced to compare mm-spaces via optimal transport [Mémoli, 2011]. Subsequent work in the machine learning literature proposed several variants to handle structured and attributed data, most notably Fused GW (FGW) [Titouan et al., 2019]. The  $Z$ -Gromov–Wasserstein ( $Z$ -GW) distance [Bauer et al., 2024] unifies these approaches by replacing the metric-valued distance function in classical GW with a general measurable pairwise relation taking values in a metric space  $(\mathcal{Z}, d_{\mathcal{Z}})$ , so that classical GW, FGW and other formulations arise as particular instances of this construction.

**Definition 3.3** ( $Z$ -networks). *Let  $(\mathcal{Z}, d_{\mathcal{Z}})$  be a metric space. A  $Z$ -network is a triple  $(\mathcal{X}, \omega_{\mathcal{X}}, \mu_{\mathcal{X}})$ , where  $\mathcal{X}$  is a measurable space,  $\mu_{\mathcal{X}}$  is a probability measure on  $\mathcal{X}$ , and  $\omega_{\mathcal{X}} : \mathcal{X} \times \mathcal{X} \rightarrow \mathcal{Z}$  is a measurable function encoding pairwise relational information. Unlike mm-spaces,  $\omega_{\mathcal{X}}$  is not required to be a metric.*

**Z-Gromov–Wasserstein distance.** Given two  $Z$ -networks  $(\mathcal{X}, \omega_{\mathcal{X}}, \mu_{\mathcal{X}})$  and  $(\mathcal{Y}, \omega_{\mathcal{Y}}, \mu_{\mathcal{Y}})$ , the  $Z$ -Gromov–Wasserstein  $p$ -distance ( $p \geq 1$ ) is defined as

$$\text{GW}_p^Z(\mathcal{X}, \mathcal{Y}) = \frac{1}{2} \inf_{\pi \in \Pi(\mu_{\mathcal{X}}, \mu_{\mathcal{Y}})} \left( \iint_{(\mathcal{X} \times \mathcal{Y})^2} d_{\mathcal{Z}}(\omega_{\mathcal{X}}(x, x'), \omega_{\mathcal{Y}}(y, y'))^p \, d\pi(x, y) \, d\pi(x', y') \right)^{1/p}. \quad (4)$$

When  $\mathcal{Z} = \mathbb{R}$  and  $\omega_{\mathcal{X}}$  is the usual metric distance ( $\omega_{\mathcal{X}} = d_{\mathcal{X}}$ ),  $\text{GW}_p^Z$  reduces to the classical GW distance.

**Definition 3.4** (Weak isomorphism [Bauer et al., 2024]). *Two  $Z$ -networks  $(\mathcal{X}, \omega_{\mathcal{X}}, \mu_{\mathcal{X}})$  and  $(\mathcal{Y}, \omega_{\mathcal{Y}}, \mu_{\mathcal{Y}})$  are said to be weakly isomorphic, written  $\mathcal{X} \sim \mathcal{Y}$ , if there exists a  $Z$ -network  $(\mathcal{W}, \omega_{\mathcal{W}}, \mu_{\mathcal{W}})$  and measure-preserving maps  $\phi_{\mathcal{X}} : \mathcal{W} \rightarrow \mathcal{X}$  and  $\phi_{\mathcal{Y}} : \mathcal{W} \rightarrow \mathcal{Y}$  such that*

$$\omega_{\mathcal{W}}(w, w') = \omega_{\mathcal{X}}(\phi_{\mathcal{X}}(w), \phi_{\mathcal{X}}(w')) = \omega_{\mathcal{Y}}(\phi_{\mathcal{Y}}(w), \phi_{\mathcal{Y}}(w'))$$

for  $\mu_{\mathcal{W}} \otimes \mu_{\mathcal{W}}$  for almost every pair  $(w, w')$ .

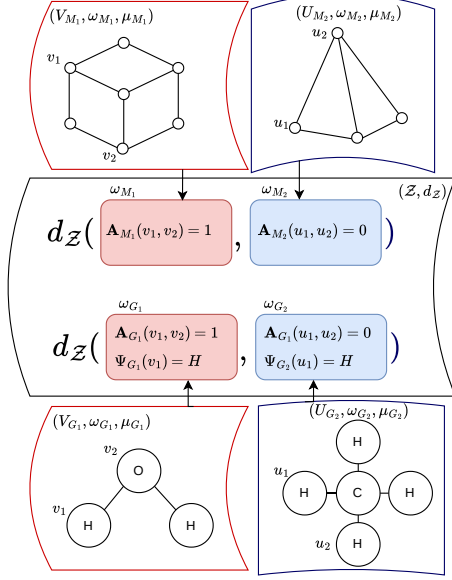


Figure 2: Z-GW distance

**Weak isomorphism and metricity.** The distance  $\text{GW}_p^Z$  defines a pseudometric on the space of  $Z$ -networks. To obtain a genuine metric, one considers equivalence classes under *weak isomorphism*. We denote by  $\mathfrak{M}$  the collection of all  $Z$ -networks  $(\mathcal{X}, \omega_{\mathcal{X}}, \mu_{\mathcal{X}})$ , and by  $\mathcal{M} := \mathfrak{M}/\sim$  the corresponding quotient space under weak isomorphism.

**Theorem 3.5** ([Bauer et al., 2024, Thm. 29]). *For any separable metric space  $(\mathcal{Z}, d_{\mathcal{Z}})$  and  $p \geq 1$ , the distance  $\text{GW}_p^Z$  induces a genuine metric on  $\mathcal{M}$ .*

**Remark 3.6** (Working with representatives in practice). *Although the quotient space  $\mathcal{M} := \mathfrak{M}/\sim$  is the natural mathematical domain on which  $\text{GW}_p^Z$  is well defined, it is not directly accessible in practice. Each element of  $\mathcal{M}$  corresponds to an equivalence class of isomorphic realizations, and any concrete representative in  $\mathfrak{M}$  is inherently arbitrary. In practical settings, observed data are therefore provided as explicit  $Z$ -networks in  $\mathfrak{M}$  (e.g., graphs, attributed graphs, or meshes), and learning algorithms operate on these representations. Consequently, both empirical datasets and prediction tasks are formulated at the level of  $\mathfrak{M}$ , while permutation-invariant losses such as  $\text{GW}_p^Z$  ensure consistency with the underlying quotient structure.*

## 4 CONFORMAL GRAPH PREDICTION

### 4.1 PROBLEM SETUP

**Graphs as  $Z$ -networks.** Graphs can be naturally viewed as finite  $Z$ -networks. Let  $G = (V, E, F)$  be a graph, where  $V$  is the node set with  $|V| = n \in \mathbb{N}^*$ ,  $E \subseteq V \times V$  is the edge set, and  $\Psi : V \rightarrow \mathbb{R}^d$  is a node feature map, with  $\Psi(i)$  denoting the feature associated to node  $i \in V$ .

We associate to  $G$  a  $Z$ -network  $(V, \omega_G, \mu_G)$ , where  $\mu_G \in \mathcal{P}(V)$  is a probability measure on  $V$  (assumed uniform in this case), and  $\omega_G : V \times V \rightarrow \mathcal{Z}$  encodes pairwise relational information between nodes. This representation provides a unified way to encode both graph structure and node attributes, enabling the comparison of graphs within the general  $Z$ -GW distance.

**Example 4.1** (Fused Network Gromov-Wasserstein Distance). *Choosing the pairwise structure  $\omega_G$  such that it combines structural and node-level information allows to retrieve the so-called Fused Network Gromov-Wasserstein Distance introduced by Yang et al. [2024]:*

$$\omega_G(i, k) = (\mathbf{A}(i, k), \mathbf{X}(i, k), \Psi(i)) \in \mathcal{Z} := \Omega \times \mathbb{R}^m \times \mathbb{R}^d,$$

where the matrix  $\mathbf{A} : V \times V \rightarrow \Omega$  defined from the set of edges  $E$  encodes graph connectivity (e.g. Adjacency, Shortest Path, Laplacian, etc),  $\mathbf{X} : V \times V \rightarrow \mathbb{R}^m$  represents edge features, and  $\Psi(i) \in \mathbb{R}^d$  denotes the feature associated to node  $i$ . For instance, when  $\mathbf{A}$  is the adjacency matrix,  $\Omega = \{0, 1\}$ . The product space  $\mathcal{Z}$  is equipped with a weighted  $\ell_q$  metric

$$d_{\mathcal{Z}}((a, x, \psi), (a', x', \psi')) = \left( \beta d_{\Omega}(a, a')^q + \gamma d_{\mathbb{R}^m}(x, x')^q + (1 - \gamma - \beta) d_{\mathbb{R}^d}(\psi, \psi')^q \right)^{1/q}, \quad (5)$$

for  $\gamma, \beta \in [0, 1]$ ,  $q \geq 1$ .

**Example 4.2** (Fused Gromov-Wasserstein Distance [Vayer et al., 2020]). *Setting  $\gamma = 0$  and  $\beta \in [0, 1]$ , we recover the Fused Gromov-Wasserstein (no more edge features).*

**Example 4.3** (Gromov-Wasserstein Distance [Mémoli, 2011]). *To retrieve Gromov-Wasserstein distance between unlabeled graphs (no more feature nodes), we set  $\gamma = 0$  and  $\beta = 1$ .*

**Discrete  $Z$ -Gromov-Wasserstein for graphs.** Let  $G_1 = (V_1, \omega_1, \mu_1)$  and  $G_2 = (V_2, \omega_2, \mu_2)$  be finite graphs with  $|V_1| = n$  and  $|V_2| = m$  and uniform measures. The discrete  $Z$ -GW distance between  $G_1$  and  $G_2$  is defined as

$$\min_{\pi \in \Pi(\mu_1, \mu_2)} \left( \sum_{i, k \in V_1} \sum_{j, l \in V_2} d_{\mathcal{Z}}(\omega_1(i, k), \omega_2(j, l))^p \pi_{ij} \pi_{kl} \right)^{1/p}. \quad (6)$$

In the finite graph setting with uniform measures, weak isomorphism admits a simple characterization (see Proposition 4.4 below). As a consequence,  $\text{GW}_p^Z$  defines a permutation-invariant distance on graphs.

**Proposition 4.4** (Weak isomorphism and permutation invariance). *Let  $(V_1, \omega_1, \mu_1)$  and  $(V_2, \omega_2, \mu_2)$  be finite  $Z$ -networks associated to  $G_1$  and  $G_2$ , respectively, with  $|V_1| = |V_2| = n$  and uniform measures  $\mu_1 = \mu_2$ . Then  $G_1 \sim_n G_2$  if and only if there exists a permutation matrix  $P \in \sigma_n$  such that  $\omega_1 = P^T \omega_2 P$ .*

From now on, we specialize the spaces  $\mathfrak{M}$  and  $\mathcal{M}$  to graphs. We denote by  $\mathfrak{M}$  the collection of all graphs with at most  $N$  nodes, i.e.  $\mathfrak{M} = \bigsqcup_{n=1}^N \mathcal{G}_n$ , in which  $\mathcal{G}_n$  are the space of all graphs with  $n$  nodes represented in a labeled form, and by  $\mathcal{M} := \bigsqcup_{n=1}^N (\mathcal{G}_n / \sim_n)$ , the union of the quotient graph spaces of size  $n$ , where graphs are identified up to node permutation. For simplicity, we note  $\mathcal{M} = \mathfrak{M} / \sim$ .

**Graph-valued prediction.** We consider a graph-valued prediction model

$$f_\theta : \mathcal{X} \rightarrow \mathfrak{M}$$

that maps inputs  $x \in \mathcal{X}$  (e.g., spectra, images, or other descriptors) to graph-valued outputs  $y \in \mathfrak{M}$ . In the remainder, we assume that this model has been learned on the training dataset  $\{(X_i, Y_i)\}_{i=1}^n$  by minimizing a loss measuring discrepancy between predicted and ground-truth graphs. Crucially, such losses must be invariant to node relabeling; the  $\text{GW}_p^Z$  distance, for instance, satisfies this requirement by construction. In the experimental part, we consider two off-the-shelves graph prediction models  $f_\theta$ : ANY2GRAPH[Krzakala et al., 2024], a general-purpose end-to-end graph predictor restricted to small-size graphs and SPECBRIDGE[Wang et al., 2026] specialized on Metabolite identification from mass spectra and based on autoencoders.

## 4.2 GENERAL FRAMEWORK FOR CONFORMAL GRAPH PREDICTION

Given the previous set up, for a given input  $x$ , we get a concrete graph  $\hat{y} = f_\theta(x) \in \mathfrak{M}$ . Uncertainty guarantees, however, must be invariant to node relabeling and are therefore stated on the quotient space  $\mathcal{M}$ .

**Assumption 4.5** (Exchangeable data). *The observed data  $(X_i, Y_i)_{i=1}^n$  are exchangeable and take values in  $\mathcal{X} \times \mathfrak{M}$ .*

**Definition 4.6** (Canonical projection). *The canonical projection  $h : \mathfrak{M} \rightarrow \mathcal{M} := \mathfrak{M} / \sim$  maps a graph  $y \in \mathfrak{M}$  to its equivalence class*

$$h(y) := [y] = \{y' \in \mathfrak{M} \mid y' \sim y\},$$

corresponding to all node relabelings of the same underlying graph.

Given a graph predictor  $f_\theta$  and representative-valued data in  $\mathfrak{M}$ , we define the nonconformity score

$$s : \mathcal{X} \times \mathfrak{M} \rightarrow \mathbb{R}_+, \quad s(x, y) := \text{GW}_p^Z(f_\theta(x), y).$$

Since  $\text{GW}_p^Z$  is invariant under node permutation, the score  $s$  is invariant under the equivalence relation  $\sim$ . As a consequence,  $s$  factors through the canonical projection  $h$  and induces a well-defined score

$$\tilde{s} : \mathcal{X} \times \mathcal{M} \rightarrow \mathbb{R}_+, \quad \tilde{s}(x, \tilde{y}) = s(x, y), \quad \tilde{y} = h(y),$$

which depends only  $\tilde{y} \in \mathcal{M}$ .

**Lemma 4.7** (Exchangeability is preserved under quotient maps). *Let  $(X_i, Y_i)_{i=1}^n$  be an exchangeable sequence of random variables taking values in  $\mathcal{X} \times \mathfrak{M}$ . Let  $h : \mathfrak{M} \rightarrow \mathcal{M} := \mathfrak{M} / \sim$  be the canonical projection onto equivalence classes, and define  $\tilde{Y}_i := h(Y_i)$ . Then the induced sequence  $(X_i, \tilde{Y}_i)_{i=1}^n$  taking values in  $\mathcal{X} \times \mathcal{M}$  is exchangeable.*

Lemma 4.7 ensures that the exchangeability of the observed data is preserved when passing from representative-valued outputs in  $\mathfrak{M}$  to their equivalence classes in the quotient space  $\mathcal{M}$ .

We now establish conformal validity for  $Z$ -GW-based conformal sets. Let  $R_i = s(X_i, Y_i)$  be the calibration scores and let  $\hat{q}_{1-\alpha}$  denote their empirical  $(1 - \alpha)$ -quantile. For a new input  $X_{n+1}$ , define

$$\mathcal{C}_\alpha^{\mathfrak{M}}(X_{n+1}) = \left\{ y \in \mathfrak{M} : \text{GW}_p^Z(f_\theta(X_{n+1}), y) \leq \hat{q}_{1-\alpha} \right\}. \quad (7)$$

**Proposition 4.8** (Conformal validity on  $\mathfrak{M}$  and  $\mathcal{M}$ ). *Let  $(X_i, Y_i)_{i=1}^n$  be exchangeable random variables taking values in  $\mathcal{X} \times \mathfrak{M}$ , and let  $f_\theta : \mathcal{X} \rightarrow \mathfrak{M}$  be a predictor. Define the nonconformity score*

$$s(x, y) := \text{GW}_p^Z(f_\theta(x), y),$$

and construct the conformal prediction set  $\mathcal{C}_\alpha^{\mathfrak{M}}(x) \subseteq \mathfrak{M}$  at level  $\alpha \in (0, 1)$  using  $\tilde{s}$ . Then the following hold:

1. (Marginal coverage)

$$\mathbb{P}(Y_{n+1} \in \mathcal{C}_\alpha^{\mathfrak{M}}(X_{n+1})) \geq 1 - \alpha.$$

2. (Well-defined on Quotient)  $\mathcal{C}_\alpha^{\mathfrak{M}}(x)$  is a union of equivalence classes and therefore induces a well-defined prediction set on the quotient space,  $\mathcal{C}_\alpha^{\mathcal{M}}(x) := h(\mathcal{C}_\alpha^{\mathfrak{M}}(x)) \subseteq \mathcal{M}$ , which satisfies

$$\mathbb{P}(h(Y_{n+1}) \in \mathcal{C}_\alpha^{\mathcal{M}}(X_{n+1})) \geq 1 - \alpha.$$

All proofs are deferred to Appendix A.

## 4.3 PRACTICAL RESTRICTIONS

The conformal set defined in Eq.7 is an implicit subset of the graph space  $\mathfrak{M}$ , specified through a membership predicate rather than explicit enumeration. For any candidate graph  $y \in \mathfrak{M}$ , membership is determined by evaluating the nonconformity score  $s(x, y)$  and comparing it to the calibrated threshold. In molecular graph domains, however,  $\mathfrak{M}$  is combinatorially large, making the explicit materialization of  $\mathcal{C}(x)$  computationally infeasible.

To obtain a finite and tractable prediction set, we intersect the implicit conformal set with an input-dependent candidate

library  $\mathcal{L}(x) \subset \mathfrak{M}$  (e.g., a metabolite database determined by a mass spectrum):

$$\mathcal{C}_{\mathcal{L}}(x) = \mathcal{C}(x) \cap \mathcal{L}(x) = \{y \in \mathcal{L}(x) : s(x, y) \leq \hat{q}_{1-\alpha}\}. \quad (8)$$

In retrieval tasks, the candidate library is typically constructed to be complete, in the sense that the ground-truth output is contained almost surely, i.e.,  $\mathbb{P}(Y_{n+1} \in \mathcal{L}(X_{n+1})) = 1$ . Under this assumption,  $\mathcal{C}_{\mathcal{L}}(x)$  coincides with the exact conformal prediction set restricted to the reduced output space  $\mathcal{L}(x)$  and therefore inherits the marginal coverage guarantee.

**Remark 4.9.** *If the ground-truth output  $Y_{n+1}$  may lie outside  $\mathcal{L}(X)$ , the coverage degrades according to the probability of library incompleteness:  $\mathbb{P}(Y_{n+1} \in \mathcal{C}_{\mathcal{L}}(X_{n+1})) \geq (1 - \alpha) - \mathbb{P}(Y_{n+1} \notin \mathcal{L}(X_{n+1}))$ .*

## 5 LOCALLY ADAPTIVE GRAPH CONFORMAL PREDICTION

Previously, we extended conformal prediction to graph-valued outputs using a single global threshold on a nonconformity score. However, a global cutoff implicitly assumes homogeneous uncertainty across inputs. In practice, this assumption is rarely satisfied: some instances are intrinsically easy, while others are highly ambiguous. A single threshold therefore tends to produce overly conservative sets for easy inputs and risks undercoverage for difficult ones.

In complex, high-dimensional, or structured output spaces (e.g. graphs, manifolds, or functional data), applying standard CQR directly in the output space  $\mathfrak{M}$  is often computationally or conceptually intractable, since conditional quantiles are not naturally defined for structured objects. To provide distribution-free *locally adaptive* guarantees in these settings, we introduce *Score Conformalized Quantile Regression* (SCQR).

**Score Conformalized Quantile Regression** Given a point predictor  $f_{\theta} : \mathcal{X} \rightarrow \mathfrak{M}$  and a nonconformity score  $s(x, y) \in \mathbb{R}$ , with  $x \in \mathcal{X}$  and  $y \in \mathfrak{M}$ . SCQR relaxes the Graph conformal prediction one-size-fits-all assumption by allowing the threshold to depend on input-dependent attributes  $\omega(x) \in \Omega$ , which capture heteroscedasticity. These attributes may be the input itself (identity map) or derived quantities reflecting its complexity, e.g. size of candidate set or pre-trained embeddings.

Concretely, we first train a quantile regression model  $\psi : \Omega \rightarrow \mathbb{R}$  using the pinball loss to estimate  $(1-\alpha)$ -conditional quantile of  $s(x, y)$  on a training set. We again compute the adaptive residuals  $E_i = s(X_i, Y_i) - \psi(\omega(X_i))$ . We then compute the empirical quantile of the residuals:  $\hat{q}_{1-\alpha} = \text{Quantile} \left( \{E_i\}_{i=1}^n, \frac{\lceil (n+1)(1-\alpha) \rceil}{n} \right)$ . For a new input  $X_{n+1}$ ,

the conformal prediction set is:

$$\mathcal{C}(X_{n+1}) = \{y \in \mathfrak{M} : s(X_{n+1}, y) \leq \psi(z(X_{n+1})) + \hat{q}_{1-\alpha}\}. \quad (9)$$

The residuals  $E_i$  may take both negative and positive values. Since  $s(x, y) \geq 0$  and  $s(x, y) = 0$  indicates perfect conformity, negative residuals correspond to examples that are easier than predicted given  $\omega(x)$ , while positive residuals indicate an underestimation of difficulty. Retaining both is essential for adaptive and non-conservative conformal calibration.

**Proposition 5.1** (Marginal Coverage Guarantee of SCQR). *Let  $\{(X_i, Y_i)\}_{i=1}^{n+1}$  be exchangeable random variables, and let  $\omega : \mathcal{X} \rightarrow \Omega$  be a deterministic feature map. Assume that the nonconformity score  $s : \mathcal{X} \times \mathfrak{M} \rightarrow \mathbb{R}$  and the quantile regression function  $\psi : \Omega \rightarrow \mathbb{R}$  are fixed measurable functions, independent of the calibration sample. Then the SCQR prediction set expressed in Eq. 9 satisfies*

$$\mathbb{P}(Y_{n+1} \in \mathcal{C}(X_{n+1})) \geq 1 - \alpha. \quad (10)$$

**Remark 5.2** (One-Sided Nature of SCQR). *Unlike the original CQR for real-valued regression which often produces two-sided intervals  $[q_{low}, q_{high}]$ , SCQR is inherently one-sided. This is because nonconformity scores are typically designed to be non-negative, where smaller values represent better fits.*

## 6 NUMERICAL EXPERIMENTS

To illustrate the general applicability of our approach, we consider both a synthetic graph prediction benchmark and a real-world metabolite retrieval task. The code will be made available. We refer to Appendix C for more details on implementations and extra results.

### 6.1 SYNTHETIC DATASET

We use the synthetic Coloring dataset Krzakala et al. [2024], consisting of pairs  $(X_i, Y_i)$  where  $X_i$  is an image encoding a graph-coloring instance and  $Y_i$  is its ground-truth graph. Nodes take one of four discrete colors (blue, green, yellow, red) and edges indicate spatial neighboring. The task is to recover the underlying graph from the image, providing a controlled benchmark for image-to-graph prediction.

**Candidate sets.** For each test instance  $(X_i, Y_i)$ , we construct the candidate set  $\mathcal{L}(x)$  by selecting all graphs in the test split that share the same node-type configuration as  $Y_i$ , i.e., the same number of blue, green, yellow, and red nodes. This yields a controlled identification problem where structurally distinct graphs share identical node statistics.

Table 1: Comparison of conformal prediction (CP) and score conformalized quantile regression (SCQR) on graph-valued outputs with finite candidate sets on Coloring dataset. Both methods are evaluated at nominal coverage level  $1 - \alpha$ , with  $\alpha = 0.1$ . Arrows indicate whether higher ( $\uparrow$ ) or lower ( $\downarrow$ ) values are preferable. Implementation details are deferred to Appendix B

Task	Z-GW distance	Method	Empirical Coverage	Conformal Set Size $\downarrow$		Candidate Set Size		Reduction % $\uparrow$		Empty rate (%) $\downarrow$
				Mean	Median	Mean	Median	Mean	Median	
Colors	FGW - Adj + FD	CP	90.2%	4	1	205	223	95.8%	98.9%	8.9%
		SCQR $ \mathcal{L}(x) $	90.3%	4	1	201	223	95.6%	98.9%	8.8%
Metabolite	FGW - Lapl + Id	CP	89.0%	24	1	159	214	77.1%	98.0%	0.0%
		SCQR $ \mathcal{L}(x) $	89.2%	37	2	161	221	75.3%	94.8%	0.0%
		SCQR DREAMS( $x$ )	89.5%	15	1	164	236	84.8%	99.1%	0.4%

**Model and protocol.** We use ANY2GRAPH Krzakala et al. [2024] as graph predictor  $f_\theta$  (82% test accuracy), trained with the PMFGW loss. We use 100k samples for training and 10k each for calibration and testing.

## 6.2 METABOLITE RETRIEVAL

We evaluate our framework on tandem mass spectrometry (MS/MS)-based metabolite identification using the benchmark *MassSpecGym* Bushuiev et al. [2024]. Each input  $x$  is an MS/MS spectrum, and the goal is to recover the underlying molecular structure from a finite candidate library.

**From spectra to graphs.** We use SPECBRIDGE Wang et al. [2026], which encodes MS/MS spectra with DREAMS Bushuiev et al. [2025] and retrieves molecules in the latent space of a frozen molecular foundation model (CHEMBERTA Ahmad et al. [2022], Chithrananda et al. [2020]). We train SPECBRIDGE exactly as in the original paper. Predicted SMILES strings are deterministically mapped to molecular graphs using RDKit Landrum et al. [2013], yielding the pipeline MS/MS  $\rightarrow$  SMILES  $\rightarrow$  Graph. Thus, we retain the graph-valued prediction setting  $f_\theta : \mathcal{X} \rightarrow \mathfrak{M}$ , in which nodes correspond to atom types.

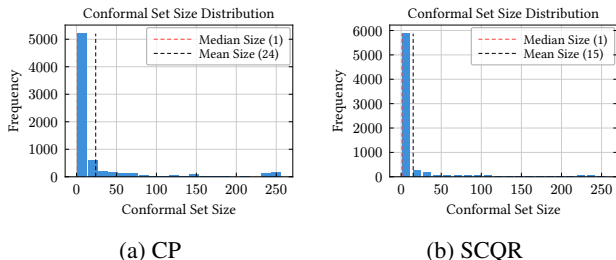


Figure 3: Conformal Set Size Histogram (MassSpecGym).

**Remark 6.1.** Our goal is to study conformal prediction in a graph-valued output space, not to improve MS/MS-to-graph models. We therefore rely on SPECBRIDGE (84.7% top-1 accuracy) as MS/MS-to-SMILES and then use RDKit, as direct MS/MS-to-graph approaches were not sufficiently

accurate on this task.

**Candidate sets.** For each spectrum  $x$ , we use the candidate library provided by *MassSpecGym*, which retrieves all molecules whose mass matches the observed spectrum and caps the set at  $|\mathcal{L}(x)| \leq 256$ . All candidates are then converted to graphs via the same deterministic mapping, yielding a finite set  $\mathcal{L}(x) \subset \mathfrak{M}$ .

## 6.3 EXPERIMENTAL PROTOCOL

**Distance and nonconformity score.** Our nonconformity score is based on the Z-GW, instantiated in practice as FGW with task-specific cost matrices. For Coloring, we use FGW with adjacency cost ( $A$ ) and Feature Diffusion (FD) initialization of the solver. For Metabolite Retrieval, we use FGW with Laplacian cost ( $L$ ) and identity initialization (Id). Complete ablations over cost matrices and initializations, are provided in Appendix C.

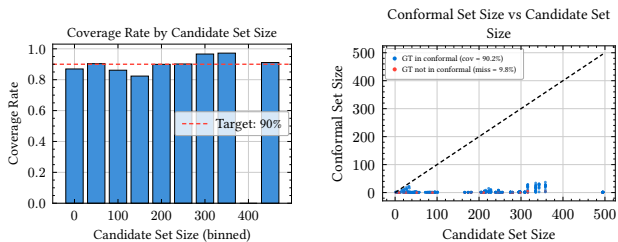
**Calibration.** Standard conformal prediction (CP) estimates a single global  $(1 - \alpha)$  quantile from the calibration set. Score-Conformalized Quantile Regression (SCQR) instead conditions the threshold on an input-dependent attribute  $\omega(x)$ . For the synthetic Coloring task, we set  $\omega(x) = |\mathcal{L}(x)|$ , i.e., the candidate set cardinality. For the metabolite retrieval task, we consider: (i)  $\omega(x) = |\mathcal{L}(x)|$ , and (ii)  $\omega(x) = \text{DREAMS}(x)$ , the learned spectral embedding of the input spectrum  $x$ .

**Evaluation metrics.** All results are reported at nominal level  $1 - \alpha = 0.9$ . We measure empirical coverage, conformal set size (mean and median), reduction relative to the full candidate library, and empty-set rate.

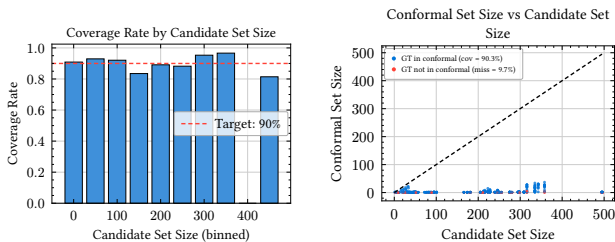
## 6.4 RESULTS

**Coverage Validity and Efficiency.** Across both tasks, empirical coverage remains close to the nominal 90%, confirming validity under Z-GW scoring, as reported in Table 1 and illustrated by the histograms in Figure 4. We evaluate

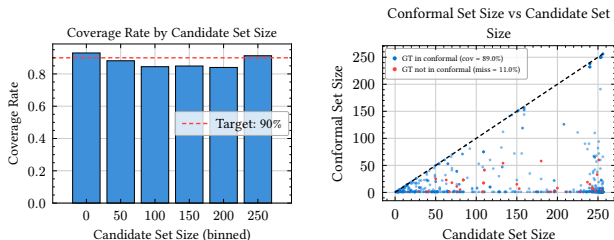
## Coloring — Conformal Prediction



## Coloring — SCQR



## Metabolite Retrieval — Conformal Prediction



## Metabolite Retrieval — SCQR

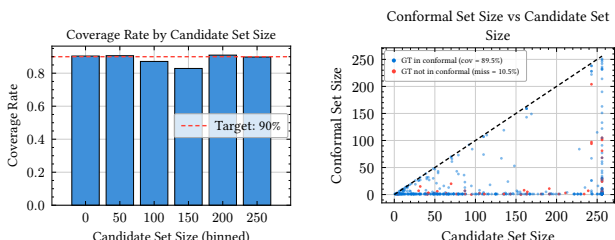


Figure 4: Conformal coverage and set size behavior across tasks. Histograms show empirical coverage versus candidate set size. Scatter plots show conformal set size versus candidate set size, the black dashed  $y = x$  line indicates no reduction, and points below the line demonstrate cases where conformal filtering reduces the set. Blue (resp. red) points indicate conformal sets containing the ground truth (resp. violations). For SCQR, the attribute function  $\omega(x)$  is task-dependent:  $\omega(x) = |\mathcal{L}(x)|$  (candidate set size) for Coloring, and  $\omega(x) = \text{DREAMS}(x)$  (mass-spectrum embedding) for Metabolite.

Table 2: Results on metabolites with a  $L$  and Id initialization

	Emp. Cov.	Conformal Set Size ↓		Reduction % ↑		Empty rate (%) ↓
		Mean	Med.	Mean	Med.	
FNGW	95.1%	44	4	63.8%	93.3%	0.0%
FGW	89.5%	15	1	84.8%	99.1%	0.4%
GW	95.0%	40	3	66.9%	94.4%	0.0%

efficiency through conformal set size and reduction relative to the candidate library. On *Coloring*, SCQR conditioned on  $|\mathcal{L}(x)|$  performs similarly to CP: the median set size is 1, with over 95% average reduction. Conditioning brings limited additional benefit in this synthetic setting. On *Metabolite Retrieval*, conditioning is crucial. SCQR based on  $|\mathcal{L}(x)|$  does not improve efficiency. In contrast, conditioning on the spectral embedding  $\text{DREAMS}(x)$  substantially reduces mean conformal set size from 24 (CP) to 15 while preserving coverage, increasing average reduction from 77.1% to 84.8%. Figure 3 shows that SCQR reduces heavy-tail behavior in conformal set sizes for metabolites.

**Versatility of  $Z$ -GW non-conformity scores.** We illustrate the versatility of the  $Z$ -GW framework by comparing several instantiations. We fix the interpolation parameters: FGW ( $\beta = 0.5$ ) and FNGW ( $\beta = \gamma = 0.33$ ). Pure GW, which only accounts for relational structure and ignores node features, naturally leads to higher uncertainty and

larger candidate sets. In contrast, FGW reduces uncertainty by incorporating finer feature-level information in addition to structure, aligning with our expectations. For FNGW, performance depends more sensitively on the balance between structural, edge feature and node feature terms.

**Top- $k$  vs Conformal.** For a fair comparison, we calibrate SCQR ( $\text{DREAMS}(x)$ ) so that its marginal coverage matches the top-5 accuracy of SPECBRIDGE (92.31%). Under this matched coverage level, the resulting conformal sets have mean size 33 and median size 1. Although half of the sets are singletons, the mean is inflated by a heavy tail. Among sets that contain the ground truth, 62.9% have size  $\leq 5$ .

## 7 CONCLUSION

We introduced a conformal prediction framework for graph-valued outputs grounded in the  $Z$ -Gromov–Wasserstein geometry. By defining nonconformity through  $Z$ -GW, the method provides distribution-free coverage guarantees while respecting the permutation-invariant structure of graphs. We further proposed Score-Conformalized Quantile Regression (SCQR), which yields adaptive prediction sets by conditioning on input-dependent signals, improving efficiency without compromising validity. More broadly, the framework extends naturally to other structured output spaces representable as  $Z$ -networks, such as meshes, point clouds, and distributions, suggesting a general geometry-aware approach to uncertainty quantification in structured prediction.

## References

- Walid Ahmad, Elana Simon, Seyone Chithrananda, Gabriel Grand, and Bharath Ramsundar. Chemberta-2: Towards chemical foundation models. *arXiv preprint arXiv:2209.01712*, 2022.
- Anastasios N Angelopoulos, Stephen Bates, et al. Conformal prediction: A gentle introduction. *Foundations and trends® in machine learning*, 16(4):494–591, 2023.
- Martin Bauer, Facundo Mémoli, Tom Needham, and Mao Nishino. The z-gromov-wasserstein distance. *arXiv preprint arXiv:2408.08233*, 2024.
- Luc Brogat-Motte, Rémi Flamary, Céline Brouard, Juho Rousu, and Florence d’Alché Buc. Learning to predict graphs with fused gromov-wasserstein barycenters. In *International Conference on Machine Learning*, pages 2321–2335. PMLR, 2022.
- Céline Brouard, Huibin Shen, Kai Dührkop, Florence d’Alché Buc, Sebastian Böcker, and Juho Rousu. Fast metabolite identification with input output kernel regression. *Bioinformatics*, 32(12):i28–i36, 2016.
- Roman Bushuiev, Anton Bushuiev, Niek F de Jonge, Adamo Young, Fleming Kretschmer, Raman Samusevich, Janne Heirman, Fei Wang, Luke Zhang, Kai Dührkop, et al. Massspecgym: A benchmark for the discovery and identification of molecules. *Advances in Neural Information Processing Systems*, 37:110010–110027, 2024.
- Roman Bushuiev, Anton Bushuiev, Raman Samusevich, Corinna Brungs, Josef Sivic, and Tomáš Pluskal. Self-supervised learning of molecular representations from millions of tandem mass spectra using dreams. *Nature Biotechnology*, pages 1–11, 2025.
- Anna Calissano, Aasa Feragen, and Simone Vantini. Graph-valued regression: Prediction of unlabelled networks in a non-euclidean graph space. *Journal of Multivariate Analysis*, 190:104950, 2022.
- Anna Calissano, Matteo Fontana, Gianluca Zeni, and Simone Vantini. Conformal prediction sets for populations of graphs. *arXiv preprint arXiv:2404.18862*, 2024.
- Seyone Chithrananda, Gabriel Grand, and Bharath Ramsundar. Chemberta: large-scale self-supervised pretraining for molecular property prediction. *arXiv preprint arXiv:2010.09885*, 2020.
- Victor Dheur, Matteo Fontana, Yorick Estievenart, Naomi Desobry, and Souhaib Ben Taieb. A unified comparative study with generalized conformity scores for multi-output conformal regression. in *Int. Conf. on Mach. Learning (ICML)*, 2025.
- Matteo Fontana, Gianluca Zeni, and Simone Vantini. Conformal prediction: a unified review of theory and new challenges. *Bernoulli*, 29(1):1–23, 2023.
- Alan Frieze and Michał Karoński. *Introduction to random graphs*. Cambridge University Press, 2015.
- Kexin Huang, Ying Jin, Emmanuel Candes, and Jure Leskovec. Uncertainty quantification over graph with conformalized graph neural networks. *Advances in Neural Information Processing Systems*, 36:26699–26721, 2023.
- Roger Koenker and Gilbert Bassett. Regression quantiles. *Econometrica: Journal of the Econometric Society*, 46(1): 33–50, 1978.
- Vladimir Kondratyev, Alexander Fishkov, Nikita Kotelevskii, Mahmoud Hegazy, Remi Flamary, Maxim Panov, and Eric Moulines. Neural optimal transport meets multivariate conformal prediction. *arXiv preprint arXiv:2509.25444*, 2025.
- Paul Krzakala, Junjie Yang, Rémi Flamary, Florence d’Alché Buc, Charlotte Laclau, and Matthieu Labeau. Any2graph: Deep end-to-end supervised graph prediction with an optimal transport loss. *Advances in Neural Information Processing Systems*, 37:101552–101588, 2024.
- Paul Krzakala, Gabriel Melo, Charlotte Laclau, Florence d’Alché Buc, and Rémi Flamary. The quest for the graph level autoencoder (grale). *Advances in Neural Information Processing Systems (NeurIPS)*, 2025.
- Greg Landrum et al. Rdkit documentation. *Release*, 1(1-79): 4, 2013.
- Robert Lunde, Elizaveta Levina, and Ji Zhu. Conformal prediction for network-assisted regression. *Journal of the American Statistical Association*, (just-accepted):1–22, 2025.
- Facundo Mémoli. Gromov–wasserstein distances and the metric approach to object matching. *Foundations of computational mathematics*, 11(4):417–487, 2011.
- Dai Hai Nguyen, Canh Hao Nguyen, and Hiroshi Mamit-suka. Recent advances and prospects of computational methods for metabolite identification: a review with emphasis on machine learning approaches. *Briefings in bioinformatics*, 20(6):2028–2043, 2019.
- Yaniv Romano, Evan Patterson, and Emmanuel Candes. Conformalized quantile regression. *Advances in neural information processing systems*, 32, 2019.
- Glenn Shafer and Vladimir Vovk. A tutorial on conformal prediction. *Journal of machine learning research*, 9(3), 2008.

- Suprosanna Shit, Rajat Koner, Bastian Wittmann, Johannes Paetzold, Ivan Ezhov, Hongwei Li, Jiazhen Pan, Sahand Sharifzadeh, Georgios Kaissis, Volker Tresp, et al. Relationformer: A unified framework for image-to-graph generation. In *European conference on computer vision*, pages 422–439. Springer, 2022.
- Gauthier Thurin, Kimia Nadjahi, and Claire Boyer. Optimal transport-based conformal prediction. *arXiv preprint arXiv:2501.18991*, 2025.
- Vayer Titouan, Nicolas Courty, Romain Tavenard, and Rémi Flamary. Optimal transport for structured data with application on graphs. In *International Conference on Machine Learning*, pages 6275–6284. PMLR, 2019.
- Titouan Vayer, Laetitia Chapel, Rémi Flamary, Romain Tavenard, and Nicolas Courty. Fused gromov-wasserstein distance for structured objects. *Algorithms*, 13(9):212, 2020.
- Vladimir Vovk, Alexander Gammerman, and Glenn Shafer. *Algorithmic learning in a random world*. Springer, 2005.
- Yinkai Wang, Yan Zhou Chen, Xiaohui Chen, Li-Ping Liu, and Soha Hassoun. Specbridge: Bridging mass spectrometry and molecular representations via cross-modal alignment. *arXiv preprint arXiv:2601.17204*, 2026.
- Junjie Yang, Matthieu Labeau, and Florence d’Alché Buc. Exploiting edge features in graph-based learning with fused network gromov-wasserstein distance. *Transactions on Machine Learning Research*, 2024.
- Botong Zhang, Shuo Li, and Osbert Bastani. Conformal structured prediction. *arXiv preprint arXiv:2410.06296*, 2024.
- Yiwen Zhang, Keyan Ding, Yihang Wu, Xiang Zhuang, Yi Yang, Qiang Zhang, and Huajun Chen. Breaking the modality barrier: Generative modeling for accurate molecule retrieval from mass spectra. *arXiv preprint arXiv:2511.06259*, 2025.

## A MORE ON THEORETICAL RESULTS

### A.1 PROOF OF PROPOSITION 4.4

*Proof.* Fix orderings  $V_1 = \{v_1, \dots, v_n\}$  and  $V_2 = \{w_1, \dots, w_n\}$  and identify  $\omega_1, \omega_2$  with their matrix representations.

( $\Rightarrow$ ) Assume  $G_1 \sim G_2$ . By Definition 3.4, there exist a finite  $Z$ -network  $W = (V_W, \omega_W, \mu_W)$  and measure-preserving maps  $\phi_1 : V_W \rightarrow V_1$  and  $\phi_2 : V_W \rightarrow V_2$  such that

$$\omega_W = \phi_1^* \omega_1 = \phi_2^* \omega_2 \quad \mu_W \otimes \mu_W\text{-a.e.}$$

Since  $\mu_1$  is uniform and measure preserving,

$$\mu_W(\phi_1^{-1}(\{v\})) = \mu_1(\{v\}) = \frac{1}{n} \quad \forall v \in V_1,$$

hence  $\phi_1$  is surjective; similarly for  $\phi_2$ . Writing  $\mu_W = \sum_{k=1}^N c_k \delta_{u_k}$  with  $c_k > 0$ , the above implies

$$\sum_{u_k: \phi_1(u_k)=v} c_k = \frac{1}{n} \quad \forall v \in V_1,$$

and analogously for  $\phi_2$ .

Since  $V_W$  is finite with full-support measure, the pullback identity holds everywhere:

$$\omega_W(u, u') = \omega_1(\phi_1(u), \phi_1(u')) = \omega_2(\phi_2(u), \phi_2(u')) \quad \forall u, u' \in V_W.$$

Choose a section  $s : V_1 \rightarrow V_W$  with  $\phi_1 \circ s = \text{id}_{V_1}$  and define  $\varphi := \phi_2 \circ s : V_1 \rightarrow V_2$ . Then

$$\omega_1(v_i, v_j) = \omega_2(\varphi(v_i), \varphi(v_j)) \quad \forall i, j,$$

so  $\omega_1 = \varphi^* \omega_2$ . Since  $\mu_1$  and  $\mu_2$  are uniform atomic measures and  $\varphi$  is measure-preserving, each fiber  $\varphi^{-1}(\{w\})$  has mass  $1/n$ . As  $|V_1| = |V_2| = n$ , this implies that all fibers are singletons and hence  $\varphi$  is bijective. Let  $P = (P_{ij}) \in \sigma_n$  be the permutation matrix defined by

$$P_{ij} := \mathbb{I}_{\{w_j = \varphi(v_i)\}},$$

so that  $\omega_1 = P^\top \omega_2 P$ .

( $\Leftarrow$ ) If  $\omega_1 = P^\top \omega_2 P$  for some  $P \in \sigma_n$ , let  $\varphi$  be the associated bijection and set  $W := G_1$ ,  $\phi_1 := \text{id}$ ,  $\phi_2 := \varphi$ . Both maps are measure-preserving and the pullback identity holds everywhere, hence  $G_1 \sim G_2$ .  $\square$

### A.2 EXTRA RESULTS FOR SECTION 4

**Lemma A.1** (Measurable maps preserve equality in distribution). *Let  $(\Omega, \mathcal{F}, \mathbb{P})$  be a probability space. Let  $Z$  and  $Z'$  be random variables taking values in a measurable space  $(\mathcal{Z}, \Sigma_{\mathcal{Z}})$ , and let  $g : \mathcal{Z} \rightarrow \mathcal{Y}$  be a measurable map into another measurable space  $(\mathcal{Y}, \Sigma_{\mathcal{Y}})$ . If*

$$Z \stackrel{d}{=} Z',$$

then

$$g(Z) \stackrel{d}{=} g(Z').$$

*Proof.* Let  $B \in \Sigma_{\mathcal{Y}}$  be arbitrary. Since  $g$  is measurable,  $g^{-1}(B) \in \Sigma_{\mathcal{Z}}$ , and therefore

$$\mathbb{P}(g(Z) \in B) = \mathbb{P}(Z \in g^{-1}(B)) = \mathbb{P}(Z' \in g^{-1}(B)) = \mathbb{P}(g(Z') \in B).$$

Since this holds for all measurable sets  $B \subseteq \mathcal{Y}$ , we conclude that  $g(Z)$  and  $g(Z')$  have the same distribution.  $\square$

### A.3 PROOF OF LEMMA 4.7

*Proof.* Exchangeability of  $(X_i, Y_i)_{i=1}^n$  means that for any permutation  $\sigma$  of  $\{1, \dots, n\}$ ,

$$(X_1, Y_1, \dots, X_n, Y_n) \stackrel{d}{=} (X_{\sigma(1)}, Y_{\sigma(1)}, \dots, X_{\sigma(n)}, Y_{\sigma(n)}).$$

Define the measurable map  $g : \mathcal{X} \times \mathfrak{M} \rightarrow \mathcal{X} \times \mathcal{M}$ ,  $g(x, y) := (x, h(y))$ . Since  $h$  is measurable, so is  $g$ . Applying  $g$  componentwise and invoking Lemma A.1, we obtain

$$(X_1, \tilde{Y}_1, \dots, X_n, \tilde{Y}_n) \stackrel{d}{=} (X_{\sigma(1)}, \tilde{Y}_{\sigma(1)}, \dots, X_{\sigma(n)}, \tilde{Y}_{\sigma(n)}),$$

where  $\tilde{Y}_i = h(Y_i)$ . Since this holds for all permutations  $\sigma$ , the sequence  $(X_i, \tilde{Y}_i)_{i=1}^n$  is exchangeable.  $\square$

### A.4 PROOF OF PROPOSITION 4.8

*Proof.* By invariance of  $s$  under  $\sim$ , it factors through the canonical projection  $h$  and induces a score on  $\mathcal{M}$ . By Lemmas A.1, the score sequence  $\{s(X_i, Y_i)\}_{i=1}^n$  is exchangeable. Standard conformal prediction theory Angelopoulos et al. [2023] then yields

$$\mathbb{P}(Y_{n+1} \in \mathcal{C}_\alpha^{\mathfrak{M}}(X_{n+1})) \geq 1 - \alpha.$$

Since  $\tilde{s}(x, h(y)) = s(x, y)$ , membership in  $\mathcal{C}_\alpha^{\mathfrak{M}}(x)$  depends only on the equivalence class  $h(y)$ . Hence, for any  $y, y' \in \mathfrak{M}$  with  $h(y) = h(y')$ ,

$$y \in \mathcal{C}_\alpha^{\mathfrak{M}}(x) \iff y' \in \mathcal{C}_\alpha^{\mathfrak{M}}(x),$$

so  $\mathcal{C}_\alpha^{\mathfrak{M}}(x)$  is a union of equivalence classes. Therefore the projection

$$\mathcal{C}_\alpha^{\mathcal{M}}(x) := h(\mathcal{C}_\alpha^{\mathfrak{M}}(x))$$

is well defined. Let  $\tilde{Y}_{n+1} := h(Y_{n+1})$  denote the pushforward random variable, whose law is the pushforward measure  $P_{\tilde{Y}_{n+1}} = h_\# P_{Y_{n+1}}$ . Then

$$\begin{aligned} \mathbb{P}(\tilde{Y}_{n+1} \in \mathcal{C}_\alpha^{\mathcal{M}}(X_{n+1})) &= \mathbb{P}(\tilde{Y}_{n+1} \in h^{-1}(\mathcal{C}_\alpha^{\mathcal{M}}(X_{n+1}))) \\ &= \mathbb{P}(\tilde{Y}_{n+1} \in \mathcal{C}_\alpha^{\mathfrak{M}}(X_{n+1})), \end{aligned}$$

where the second equality follows from the fact that  $h^{-1}(\mathcal{C}_\alpha^{\mathcal{M}}(x)) = \mathcal{C}_\alpha^{\mathfrak{M}}(x)$ . Combining with the conformal coverage guarantee in  $\mathfrak{M}$  yields  $\mathbb{P}(\tilde{Y}_{n+1} \in \mathcal{C}_\alpha^{\mathcal{M}}(X_{n+1})) \geq 1 - \alpha$ .  $\square$

### A.5 PROOF OF PROPOSITION 5.1

*Proof.* Define the nonconformity scores (meta-scores) as  $E_i = s(X_i, Y_i) - \psi(\omega(X_i))$  for  $i = 1, \dots, n+1$ . Under the assumption that  $(X_i, Y_i)$  are exchangeable and that the functions  $s$ ,  $\omega$ , and  $\psi$  are measurable and independent of the calibration data, the sequence of scores  $\{E_1, \dots, E_{n+1}\}$  is also exchangeable.

Let  $E_{(1)} \leq E_{(2)} \leq \dots \leq E_{(n)}$  denote the sorted nonconformity scores of the calibration set. The threshold  $\hat{q}_{1-\alpha}$  is defined as the  $k$ -th smallest value:

$$\hat{q}_{1-\alpha} = E_{(k)}, \quad \text{where } k = \lceil (n+1)(1-\alpha) \rceil. \quad (11)$$

By the property of exchangeable random variables, the rank of  $E_{n+1}$  among the set  $\{E_1, \dots, E_{n+1}\}$  is uniformly distributed over  $\{1, \dots, n+1\}$ . Thus, the probability that the test score  $E_{n+1}$  ranks among the  $k$  smallest of the  $n+1$  total scores is:

$$\mathbb{P}(E_{n+1} \leq \hat{q}_{1-\alpha}) = \frac{k}{n+1} = \frac{\lceil (n+1)(1-\alpha) \rceil}{n+1} \geq 1 - \alpha. \quad (12)$$

Since  $Y_{n+1} \in \mathcal{C}(X_{n+1}) \iff E_{n+1} \leq \hat{q}_{1-\alpha}$ , the marginal coverage guarantee follows directly.  $\square$

## B EVALUATION METRICS

This appendix details the metrics reported in Table 1 for comparing conformal prediction (CP) and score-conditional quantile regression (SCQR) on graph-valued outputs with finite candidate sets.

**Setup.** For each test input  $x$ , let  $\mathcal{L}(x)$  denote the associated candidate set of graphs, and let  $\mathcal{C}_\alpha(x) \subseteq \mathcal{L}(x)$  be the conformal prediction set constructed at nominal coverage level  $1 - \alpha$ . Let  $y$  denote the ground-truth graph.

**Empirical Coverage.** Empirical coverage is computed as

$$\widehat{\text{Cov}}(1 - \alpha) = \frac{1}{|\mathcal{D}_{\text{test}}|} \sum_{(x,y) \in \mathcal{D}_{\text{test}}} \mathbb{I}\{y \in \mathcal{C}_\alpha(x)\}.$$

Both CP and SCQR are evaluated at the same nominal level  $1 - \alpha$ .

**Prediction Set Size.** The prediction set size for an input  $x$  is given by  $|\mathcal{C}_\alpha(x)|$ . We report both the mean and the median of this quantity across the test set to account for potential skewness in the distribution of set sizes.

**Relative Reduction.** To quantify efficiency relative to the original candidate set, we define the relative reduction for each input as

$$\text{Reduction}(x) = \frac{|\mathcal{L}(x)| - |\mathcal{C}_\alpha(x)|}{|\mathcal{L}(x)|} \times 100\%.$$

We report the mean and median reduction over the test set.

**Empty Set Rate.** The empty set rate is defined as

$$\frac{1}{|\mathcal{D}_{\text{test}}|} \sum_{(x,y) \in \mathcal{D}_{\text{test}}} \mathbb{I}\{\mathcal{C}_\alpha(x) = \emptyset\}.$$

This quantity reflects how often the conformal procedure returns no candidate graph and is reported as a sanity check in finite-candidate settings.

**Remark B.1.** *Reporting both mean and median statistics is crucial due to the typically heavy-tailed distribution of candidate set sizes. While both CP and SCQR are guaranteed to satisfy marginal coverage, differences in set size and reduction reflect their relative efficiency, with SCQR expected to yield more adaptive prediction sets.*

**Remark B.2.** *We distinguish between validity, defined as marginal coverage, and efficiency, defined as the size of the conformal prediction set. Since prediction set size is meaningful only when the ground truth is contained in the conformal set, we report mean and median **prediction set size** and **relative reduction** conditioned on coverage, i.e., over the subset*

$$\{x \mid (x, y) \in \mathcal{D}_{\text{test}}, y \in \mathcal{C}_\alpha(x)\}.$$

*As a consequence, the reported candidate set statistics in Table 1 may differ across methods, since they are computed only over the subset of inputs for which the conformal set contains the ground truth. Because each method achieves coverage on slightly different instances, the corresponding candidate set averages are evaluated on different subsets. Coverage itself is always reported over the full test set.*

## C EXPERIMENTAL DETAILS

### C.1 DATASETS

We describe here the datasets and evaluation protocols used for the Coloring and Metabolite Retrieval tasks.

**Metabolite Retrieval.** For the metabolite identification task, we use the *MassSpecGym* dataset Bushuiev et al. [2024]. The test fold was randomly split into a calibration set (60%) and a validation set (40%). The split was done using `numpy.random(len(dataset))` with a seed of 42, all values under 0.6 going to the calibration split.

Conformal calibration was performed on the calibration set, and all reported metrics were computed on the validation set.

**Coloring (Synthetic).** For the Coloring task, we use the synthetic dataset introduced in Krzakala et al. [2024]. The dataset already provides predefined test and validation splits, in which we used 10k for each. We use the test split for conformal calibration and report all evaluation metrics on the validation split.

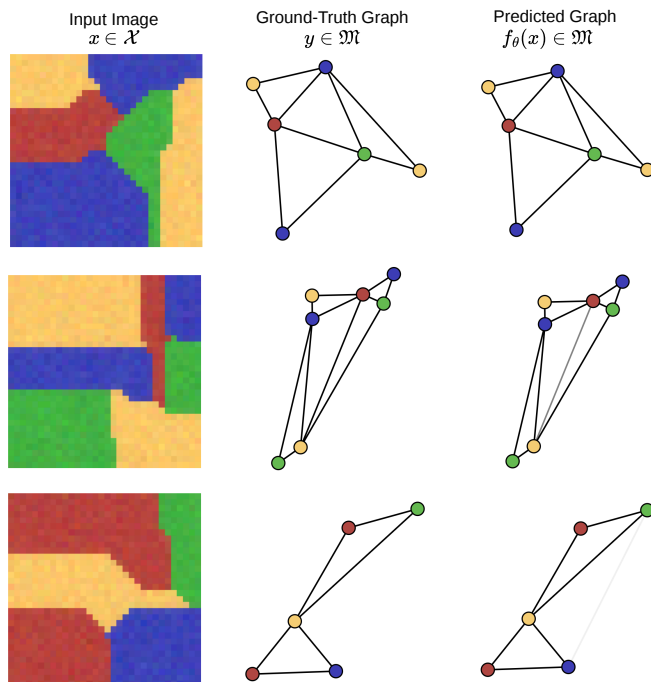


Figure 5: Coloring dataset examples using ANY2GRAPH as graph predictor.

### C.2 TRAINING

For the Coloring task, we use ANY2GRAPH Krzakala et al. [2024], and for the Metabolite Retrieval task, we use SPECBRIDGE Wang et al. [2026]. Both models were trained using the default configurations provided in their respective official repositories, without additional hyperparameter tuning.

Training was performed on NVIDIA A100 GPU. Conformal calibration and evaluation were conducted on CPU.

SCQR calibration based on candidate set size  $|\mathcal{L}(x)|$  was done by fitting a linear quantile regressor to predict calibration set non-conformity scores from  $|\mathcal{L}(x)|$ .

SCQR calibration based on DREAMS embeddings was done by training a 2-layer neural network to predict non-conformity scores from them.

The architecture is as follows:

- Linear (768, 384)
- ReLU
- Linear (384, 1)

The network was trained with the following parameters:

Table 3: embedding-based SCQR neural network training parameters

Parameter	Value
Optimizer	Adam
Learning rate	0.001
Batch size	32
Early stopping patience	3
Early stopping minimum loss improvement	0.0001

Complete training on the 10 000 samples of the calibration set takes a few seconds.

### C.3 COMPLETE RESULTS

We report here the full set of quantitative results for all experimental configurations. These tables provide the complete numerical evaluation corresponding to the summary results presented in the main paper. All the FGW variants were instantiated with  $\beta = 0.5$ .

Table 4: Comparison of conformal prediction (CP) and score-conditional quantile regression (SCQR) on graph-valued outputs with finite candidate sets on Coloring dataset. Both methods are evaluated at nominal coverage level  $1 - \alpha$ , with  $\alpha = 0.1$ . Arrows indicate whether higher ( $\uparrow$ ) or lower ( $\downarrow$ ) values are preferable.

Task	Z-GW distance	C	$G_0$	Method	Empirical Coverage	Mean set size $\downarrow$	Median set size $\downarrow$	Mean reduction (%) $\uparrow$	Median reduction (%) $\uparrow$	Empty rate (%) $\downarrow$
Colors	FGW	A	FD	CP	90.2%	4	1	95.8%	98.9%	9.0%
		A	FD	SCQR $ \mathcal{L}(x) $	90.3%	4	1	95.6%	98.9%	8.8%
	FGW	A	Id	CP	90.4%	6	2	94.4%	97.9%	5.1%
Metabolite	FGW	L	Id	CP	89.0%	24	1	77.1%	98.0%	0.0%
		L	Id	SCQR $ \mathcal{L}(x) $	89.2%	37	2	75.3%	94.8%	0.0%
		L	Id	SCQR DREAMS( $x$ )	89.5%	15	1	84.8%	99.1%	0.4%
	FGW $k = 2$	L	Id	CP	89.7%	30	1	74.3%	96.0%	0.0%
		L	Id	CP	89.5%	35	9	65.4%	87.2%	0.0%
	FGW $\lambda = 1$	L	LFD	CP	89.6%	39	13	68.3%	83.3%	0.0%
		L	Id	CP	89.7%	42	15	66.5%	79.7%	0.0%
	FGW diff	L	Id	CP	89.5%	43	13	65.6%	80.4%	0.0%
		L	FD	CP	89.6%	52	30	59.4%	70.0%	0.0%
	FGW	SP	Id	CP	89.6%	56	41	59.5%	63.5%	0.0%

### C.4 RESULTS BY HYPERPARAMETER

We report here additional experiments evaluating the effect of raising the cost matrix to power  $k$ , and of different cost matrices and FGW  $G_0$  priors.

**Fixed hyperparameters.** Unless stated otherwise, the following configuration is used:

- **Task:** Metabolite Retrieval.
- **Cost matrix:** Graph Laplacian (selected based on strongest empirical performance and more interpretable matrix powers).
- **FGW prior:** Identity initialization (best empirical performance on this task).

Table 5: Summary of acronyms used in the experiments.

Category	Acronym	Description
Cost Matrix $C$	$A$	Adjacency
	$L$	Laplacian
	$L^{sym}$	Laplacian (symmetrically normalized)
	$SP$	Shortest Paths
Initial Transport Plan $G_0$	FD	<b>Feature Diffusion:</b> Solution to the <i>Earth Mover's Distance</i> problem for given nodes of feature augmented vector $(F, AF)$
	LFD	<b>Laplacian Feature Diffusion:</b> Same as Feature Diffusion but with features $(F, LF)$
	LFD-sym	<b>Sym-Norm Laplacian Feature Diffusion:</b> Same as Feature Diffusion but with features $(F, L^{sym}F)$
	Id	<b>Identity matrix:</b> when the two graphs have the same amount of nodes, else use the solver's default initialization.
	Uniform	<b>Uniform:</b> FGW solver default initialization (uniform transport).
Z-GW distance	$k$	The cost matrix is put to the power of $k$
	$\lambda$	The cost matrix is put to the exponential: $\exp(-\lambda M)$
	diff	The node feature matrix is diffused once by multiplying by the cost matrix

Table 6: Cost matrix powers, without diffusion

k	Empirical Coverage	Mean set size ↓	Median set size ↓	Mean reduction (%) ↑	Median reduction (%) ↑	Empty rate (%) ↓
1	89.2%	24	1	77.1%	97.8%	0.0%
2	89.7%	30	1	74.4%	96.0%	0.0%
3	89.3%	34	1	71.5%	93.8%	0.0%
4	89.7%	37	2	69.7%	92.3%	0.0%
5	89.8%	37	2	70.1%	92.2%	0.0%

We vary the exponent  $k$  while keeping all other parameters fixed and report the corresponding results below.

The choices of the  $G_0$  FGW prior transport and of the cost matrix both influence the speed of convergence and the performance of the produced distances for conformal set prediction.

Table 7: Cost matrix powers, **with** feature diffusion (feature matrix is multiplied by  $L^k$ )

k	Empirical Coverage	Mean set size ↓	Median set size ↓	Mean reduction (%) ↑	Median reduction (%) ↑	Empty rate (%) ↓
1	89.7%	41	15	66.5%	80.0%	0.0%
2	89.4%	35	10	69.5%	86.6%	0.0%
3	89.5%	35	9	69.5%	86.8%	0.0%
4	89.4%	37	10	68.8%	85.6%	0.0%
5	89.5%	38	10	68.5%	84.4%	0.0%

Table 8: Cost matrix impact on different tasks. The metabolites task uses the identity  $G_0$  prior while the colors task uses the feature diffusion  $G_0$  prior. For metabolites, the FGW computation does not converge in a reasonable amount of time with the adjacency cost matrix.

Task	Cost Matrix	Empirical Coverage	Mean set size ↓	Median set size ↓	Mean reduction (%) ↑	Median reduction (%) ↑	Empty rate (%) ↓
Metabolites	$L$	89.0%	24	1	77.1%	98.0%	0.0%
	$L^{sym}$	89.4%	31	5	68.9%	93.1%	0.0%
	$A$	89.6%	30	7	68.1%	90.4%	0.0%
	$SP$	89.6%	56	41	59.5%	63.5%	0.0%
Colors	$A$	90.2%	4	1	95.8%	98.9%	9.0%
	$L^{sym}$	90.4%	4	1	95.8%	98.9%	8.5%
	$L$	90.8%	4	1	95.5%	98.7%	8.3%
	$SP$	90.1%	205	223	2.2%	0.0%	2.6%

Table 9:  $G_0$  prior impact on different tasks. The metabolites task uses the laplacian cost matrix, while the colors task uses the adjacency cost matrix. Note that uniform  $G_0$  prior often converges very slowly.

Task	$G_0$	Empirical Coverage	Mean set size ↓	Median set size ↓	Mean reduction (%) ↑	Median reduction (%) ↑	Empty rate (%) ↓
Metabolites	Id	89.0%	24	1	77.1%	98.0%	0.0%
	LFD-sym	89.5%	37	10	69.0%	86.2%	0.0%
	LFD	89.6%	39	13	68.3%	83.3%	0.0%
	FD	89.6%	52	30	59.4%	70.0%	0.0%
	Uniform	89.4%	140	149	5.8%	0.4%	0.5%
Colors	LFD	90.4%	4	1	95.8%	98.9%	8.7%
	FD	90.2%	4	1	95.8%	98.9%	9.0%
	Uniform	90.1%	4	1	95.8%	98.9%	8.7%
	LFD-sym	90.0%	4	1	95.8%	98.9%	8.8%
	Id	90.4%	6	2	94.4%	97.9%	5.1%